Article

Not peer-reviewed version

3D Printing of Personalised Carvedilol Tablets Using Selective Laser Sintering

Dennis Douroumis *, Atabak Ghanizadeh Tabriz, Quentin Gonot-Munck, Arnaud Baudoux, Vivek Garg, Richard Farnish, Orestis Katsamenis, Hui Ho-Wah, Nathan Boersen, Sandra Roberts, John Jones

Posted Date: 5 July 2023

doi: 10.20944/preprints202307.0202.v1

Keywords: 3D printing; selective laser sintering; personalised medicines; oral; carvedilol

Article

3D Printing of Personalised Carvedilol Tablets Using Selective Laser Sintering

Atabak Ghanizadeh Tabriz [1,2], Quentin Gonot-Munck [4], Arnaud Baudoux [4], Vivek Garg [3], Richard Farnish [3], Orestis L. Katsamenis [7], Ho-Wah Hui [5], Nathan Boersen [5], Sandra Roberts [5], John Jones [6] and Dennis Douroumis [1,2,*]

1 Delta Pharmaceutics Ltd., Chatham, Kent ME4 4TB, UK
2 CRI Centre for Research Innovation, University of Greenwich, Chatham Maritime Kent, ME4 4TB, UK
3 The Wolfson Centre for Bulk Solids Handling Technology, Faculty of Engineering and Science University of Greenwich, Chatham ME4 4TB, UK
4 Institute of Technology in Measurements and Instrumentation, University of Rouen, Mont Saint Aignan, France
5 Drug Product Development, Bristol Myers Squibb, 556 Morris Avenue, Summit, NJ 07901, USA
6 Bristol Myers Squibb, Reeds Lane, Moreton, Wirral
7 μ-VIS X-ray Imaging Centre, Faculty of Engineering and Physical Sciences, University of Southampton, Southampton, SO17 1BJ, United Kingdom
* Correspondence: d.douroumis@gre.ac.uk

Abstract: Selective laser sintering (SLS) has drawn attention for the fabrication of three-dimensional oral dosage forms due to the plurality of drug formulations that can be processed. The aim of this work was to employ SLS with a CO_2 laser for the manufacturing of carvedilol personalised dosage forms of various strengths. Carvedilol (CVD) and vinylpyrrolidone-vinyl acetate copolymer (Kollidon VA64) blends of various ratios were sintered to produce CVD tablets of 3.125, 6.25 and 12.5 mg. The tuning of the SLS processing parameter laser intensity, improved printability and impacted the tablet hardness, friability, CVD dissolution rate, and the total amount of drug released. Physicochemical characterization showed the presence of CVD in the amorphous state. X-ray micro-CT analysis demonstrated that the applied CO_2 intensity affected the total tablet porosity, which was reduced with increased laser intensity. The study demonstrated that SLS is a suitable technology for the development of personalised medicines that meet the required specifications and patient needs.

Keywords: 3D printing; selective laser sintering; personalised medicines; oral; carvedilol

1. Introduction

3D printing has transformed manufacturing capabilities due to its widespread applications in automotive [1], biomedical [2], aerospace [3], pharmaceutical [4], and art [5]. Over the past decade there is a growing interest in the use of 3D printing technologies for pharmaceutical applications, and particularly for the design and fabrication of personalised medicines at the point of care. A wide range of 3D printing techniques such as fused deposition modelling (FDM) [6–8], material jetting (MJ) [9], selective laser sintering/melting (SLS/SLM) [10] , Stereolithography (SLA) [11], micro extrusion [12,13] and/or combination thereof [14] have been employed in pharmaceutical research.

Despite the small scale capabilities, 3D printing presents several advantages over conventional tableting including the fabrication of dosages with tailored drug amounts, size, shape and complex geometries with specific release profiles [15,16]. Hence, 3D printed dosage forms can be used for designing individualised patient treatment that meet clinical needs, improve patient compliance, and treatment of diseases [17]. The versatility of 3D printing technologies is evident by the numerous studies such as the development of paediatric chewable formulations [18,19], bilayer tablets [20], polypills [21,22] or even orally disintegrating tablets [23].

 doi:10.20944/preprints202307.0202.v1

FDM is the most frequently used printing technology for the development of complex tablet designs or compartmental dosage forms with tuneable drug dissolution rates. Nevertheless, FDM largely depends on the extrudability of pharma grade thermoplastic polymers, APIs and the printability of the formed API loaded filaments, while drug loading can also be a limiting factor [24–26]. Regardless of the numerous 3D printing applications in the design of oral solid dosage forms, the use of SLS/SLM technologies for pharmaceutical applications has not been fully exploited. In SLS/SLM technologies, the printing chamber and the powder reservoir of an SLS printer are both heated to a temperature below the melting point (T_m) or the glass transition (T_g) of the printable powder. The top layer of powder in the preheated printing chamber is then exposed to a high-power X-Y axis laser beam, which starts to sinter a predetermined 2D pattern in accordance with the product design. The process is repeated, and another thin layer of powder is dispersed once each layer has been successfully completed. The printing is attained by lowering the printing chamber to a predetermined height and rising the reservoir chamber to a predetermined height. The recoating roller/blade can then apply a fresh powder surface on top of the completed layer. A major advantage of SLS is the reduced number of processing steps (e.g., milling) and excipients in comparison to other printing technologies. Those features render SLS simpler, inexpensive and flexible with reduced processing times and material losses. Most importantly, its operational simplicity and small footprint renders SLS an appealing printing technology for point of care applications [13].

Fina et al. used SLS to investigate the printing of Kollicoat IR and Eudragit L100-55 of paracetamol formulations at 5%, 20%, and 35% loadings by weight. The blends were processed at various intensities to avoid drug degradation with the addition of 3% by weight Candurin^{â} gold sheen [27]. Depending on laser intensity, the produced paracetamol tablets featured various release profiles due to the different tablet porosities obtain for the two polymers. In another study, the printability of paracetamol tablets with polyethylene oxide, Eudragit (L100-55 and RL) and ethyl cellulose was systematically investigated. The experimental findings revealed that the paracetamol release varied based on the polymer grade, laser scanning speed, and tablet's designed shape such as solid cylindrical, gyroid and bilayer structure [28]. However, the major disadvantage of these studies was the inadequate paracetamol amounts in printed printles and the slow dissolution rates that didn't comply with pharmacopeia standards.

Recently Gueche et al [29] investigated the printing of paracetamol with Kollidon VA64/polyamide 12 blends for the formation of fast disintegrating dosage forms using a SLS printer equipped with a CO_2 laser printer. The use of different paracetamol grades with large and plate-like particles or thin and needle-like particles affected the porosity and the dissolution rates of the sintered tablets. In addition, the drug/polymer ratio, the drug loading and the particle size were found to be key critical material parameters.

To our knowledge there are no reported studies using SLS for the development of personalised dosage forms. Therefore, the aim of the work was to investigate the print-on-demand capabilities of SLS technology for developing personalised dosage forms that meet pharmacopeia specifications in terms of strength, friability, active dose, and dissolution rates. Carvedilol is used to treat heart failure and hypertension; it was selected as the model drug substance. Printing process parameters were optimized for loadings of 3.125, 6.25 and 12.5 mg respectively.

2. Materials and Methods

2.1. Materials

Kollidon VA 64 (VA64) was kindly donated by BASF (BASF-Germany) and carvedilol (CVD) was purchased from Tokyo Chemicals (Japan).

2.2. 3D Printing blend preparation

Physical blends of VA64 and CVD were prepared at two ratios of 96.875/3.125 and 93.75/6.25 weight percent respectively. The physical blends were mixed using a turbula shaker-mixer (Glen Mills T2F Shaker/Mixer, USA) at 72 rpm for 10 minutes to ensure blend homogeneity.

Preprints (www.preprints.org) | NOT PEER-REVIEWED | Posted: 5 July 2023 doi:10.20944/preprints202307.0202.v1

2.3. Thermal Gravimetric Analysis (TGA)

TGA (TGA Q5000 Thermal instruments, USA) was utilised to investigate the thermal stability of bulk materials. Approximately 2-2.5 mg of polymer and the API samples were carefully weighed and placed in to a standard 40 uL aluminium pan. The samples were heated from 25°C to 400 °C at a heating rate of 10 °C/min. The extracted raw data were analysed via TA Universal Analysis software (Universal Analysis 2000, version 4.5A, TA instruments, USA).

2.4. Differential Scanning Calorimetry (DSC)

DSC (Mettler-Toledo 823e, Switzerland) was used to evaluate the thermal behaviour of the bulk materials and the 3D printed tablets as well as an investigation of the physical state of the CVD within the 3D printed tablets. Bulk materials and a section of the 3D printed tablets were carefully weighed. Approximately 2-2.5 mg of material was placed into a 40 µL aluminium pan and crimped promptly. The CVD and the 3D printed samples were heated from 25 °C to 160 °C at a heating rate of 10 °C/min. VA64 was heated from -22 °C to 250 °C at a heating rate of 10 °C/min. The extracted DSC thermograms of bulk materials and the 3D printed tablets were analysed through STARe Excellence Thermal Analysis Software (Mettler Toledo, Switzerland).

2.5. Powder blend characterisation

2.5.1. Particle size distribution

A Mastersizer 2000 (Malvern Panalytical, UK) was utilised to investigate the particle size distribution of the blend. The experiment was performed in triplicate.

2.5.2. Flowability test (bulk and tapped density)

The Carr's Index, I, of the 3D printing blend was investigated by measuring the tapped and bulk densities of the powder. After the bulk density was measured using a 250 mL graduated cylinder, the powder was subjected to 1250 taps using a tapped density tester (Copley, JVi Series- Model JV 200i, UK) according to USP2 standards. The Carr's Index of the blend was calculated using the following equation:

$$I = 1\text{-}(V\text{-}V_0) \times 100 \quad (1)$$

where I is the Carr's index, V_0 and V are the initial and final (tapped) powder volume of the blend in the measuring cylinder, respectively.

2.6. Design and 3D printing of tablets

Several cylindrical tablet designs were created via SolidWorks software (Dassault Systems, USA) and converted into = stl files. The stl files were then transferred into an open-source slicing software Slic3r which generated the printing path (G-codes) readable by the printer. The layer height of each slice was set to 0.2 mm. Tablets were printed using a SnowWhite SLS printer (SHAREBOT, Italy) equipped with a 14 W CO_2 laser. The physical blend was then placed into both feed beds and the print bed. Several horizontal movements of the re-coater ensured refreshment of the smooth powder surface prior to printing. The blend and the environment temperature were increased to 90 °C and remained stable throughout the printing process. The waiting time, scanning speed, and end environment temperature were set at 15 min, 8,000 pps and 90 °C for all experiments. The printing processing parameters are shown in Table 1.

Table 1. CVD content, tablet dimensions, and printing processing parameters.

No	CVD (%)	Diameter (mm)	Thickness (mm)	Intensity (%)	Designed tablet weight (mg)
F1	3.125	10	4.0	25	100
F2	3.125	10	2.4	40	100

Preprints (www.preprints.org) | NOT PEER-REVIEWED | Posted: 5 July 2023 doi:10.20944/preprints202307.0202.v1

F3	3.125	10	2.2	55	100
F4	6.25	10	8.2	25	200
F5	6.25	10	4.8	40	200
F6	6.25	10	4.4	55	200
F7	12.5	10	9.4	40	400
F8	12.5	10	8.4	55	400
F9	6.25	10	4.0	25	400
F10	6.25	10	2.4	40	200
F11	6.25	10	2.2	55	200
F12	12.5	13	2.4	25	400
F13	12.5	13	1.6	40	400
F14	12.5	13	1.4	55	400

2.7. Characterisation of 3D printed tablets

2.7.1. Hardness test

The breaking force of six 3D printed tablets was measured using a Schleuniger 5Y Tablet hardness tester (Pharmatron, Netherlands).

2.7.2. Friability test

Twenty 3D printed CVD tablets were weighed and carefully placed into an EF-2L fibrillatory apparatus (ELECTROLAB, India). The rotational speed was set to 25 rpm for 4 min. After 100 drops, the weight of the tablets was recorded and the friability was calculated using the following equation:

$$F = ((W_i - W_f)/W_i) \times 100 \quad (2)$$

where F is the friability, W_i is the initial weight of the tablets, and W_f is the final weight of the tablets after the friability test.

2.7.3. Scanning Electron Microscopy (SEM)

SEM (Hitachi SU8030, Japan) was utilised to investigate internal microstructures of the 3D printed tablets as well as the laser intensity effect on tablet porosity and permeability. Tablets were kept secured on an aluminium stub with a conductive carbon adhesive tape (Agar Scientific, Stansted, UK). The tablets were then examined vis SEM and images were captured by an electron beam accelerating voltage of 1KV and magnification of 30x.

2.7.4. Weight variation

Ten 3D printed tablets were carefully weighed using an analytical scale (XSR Analytical Balance, Mettler Toledo, Switzerland). The average weight and percentage of weight variation was then calculated.

2.8. X-ray powder diffraction (XRD)

XRD was performed to determine the physical state of the bulk materials and the CVD within the tablets after 3D printing. XRD data were collected using a D8 Advance X-ray Diffractometer (Bruker AXS, Germany) equipped with a LynxEye silicon strip position sensitive detector and parallel beam optics. The diffractometer was operated with transmission geometry using Cu Kα radiation at 40 kV and 40 mA. The instrument was computer controlled using XRD commander software (Version 2.6.1, Bruker AXS, Germany) and the data was analysed using the EVA software (version 5.2.0.3, Bruker AXS, Germany). Samples were placed between foils of 2.5 μm thick mylar for measurement. Data was collected between 5 – 60° 2θ with a step size of 0.04° and a counting time of 0.2 seconds per step.

2.9. Microfocus Computed Tomography (μCT)

The micro- and macro-porosity of representative 3D printed tablets at 25%, 40% and 55% laser intensities was measured. SLS printed components were also characterized by means of X-ray microfocus computed tomography (μCT). Imaging was performed at the University of Southampton, μ-VIS X-ray Imaging Centre (www.muvis.org) using a customised μCT scanner optimised for 3D X-ray histology (www.xrayhistology.org). The system, which is based on a Nikon's XTH225ST system (Nikon Metrology UK Ltd) was operated at 110 kVp / 73 μA (8 W) without any beam pre-filtration. The source to detector and source to object distances were 906.7 mm and 30.2 mm respectively, resulting in a geometric magnification of 30x and a voxel edge size of 10 μm. The 2850 x 2850 dexels detector was binned 2x resulting in a virtual detector of 1425 x 1425 dexels. Imaging parameters were as follows: 2001 projections were collected over the 360° rotation, with 4 frames per projection being averaged for each projection to improve the signal to noise ratio.

Reconstructed data were visualised and analysed using Dragonfly software (v. 2022.1.0.1231; Object Research Systems (ORS) Inc, Montreal, Canada, 2020; software available at http://www.theobjects.com/dragonfly). The micro- and macro-pores were segmented using thresholding and manual refinement. The porosity analysis was conducted using the connected components tool applied on the segmented pores volume. The porosity percentage was calculated as the ratio between "closed and filled" volume of the object and the total volume of the pores; that is (microporosity volume / "closed and filled" volume), (macroporosity volume / "closed and filled" volume), (Total porosity (micro + macro) volume / "closed and filled" volume). "Closed and filled" volume refers to the object volume resulting by the morphologically closed binary mask of the object, followed by filling all internal "voids". This process captures the space occupied by the object including the pore space

2.10. In vitro dissolution

In vitro dissolution studies were carried out to investigate the release of CVD from the 3D printed tablets. The release studies were carried out following pharmacopeia guidelines using a Varian 705DS (Varian, USA) dissolution system, attached with a paddle apparatus. Release studies were performed at 37 ± 0.4 ◦C using 900 mL of 0.7% HCl media adjusted to pH 1.45 using 50% (w/w) sodium hydroxide. Paddle rotational speed was set to 50 rpm. Three mL of sample media was collected at 5, 10, 20, 30, 45 and 60-minute timepoints. The same volume of fresh media was added to each vessel to maintain a constant volume of dissolution media during the release study. The collected samples were then filtered using a 0.2 μm disk. All release studies for the 3D printed tablets were performed in triplicates.

2.11. UV spectroscopy

All CVD samples were analysed using UV (Lambda 365, PerkinElmer, USA) meter with 10 mm matched quartz cell to measure absorbance of solution at 247.5 nm [30]. The standard and sample solutions were prepared in distilled water. Calibration curves were made in the range of 1-15μg/ml (R^2=0.999)

3. Results and Discussion

The primary aim of this work was to implement SLS printing technology for the development of personalised dosage forms with the required CVD dose, and to meet the pharmacopeia specifications for recommended CVD release time. Furthermore, the SLS printing process was optimized to ensure that the produced tablets would present adequate strength, friability, and weight variability. SLS could be used as an onsite printing technology for point of care service that meets specific patient needs, and to help improved clinical outcomes. Prior to 3D printing optimization, the CVD/VA64 blends were characterized in terms of their thermal properties, particle size distribution, and particle morphology, which are considered critical material parameters for the printing of SLS tablets.

Preprints (www.preprints.org) | NOT PEER-REVIEWED | Posted: 5 July 2023 doi:10.20944/preprints202307.0202.v1

3.1. Thermal analysis of plain polymers

TGA experiments were carried out to evaluate the thermal stability of the bulk CVD and VA64 powder. The powder particles can achieve high temperatures during SLS printing. These temperatures may vary based on powder features. As shown in Figure 1, VA64 presented an initial mass loss of 6% due to moisture content and remained thermally stable up to 290 °C followed by a rapid mass loss due to polymer degradation. CVD showed no moisture content and was stable up to 290 °C, followed by a rapid mass loss due as a result of degradation caused by the high temperature [31].

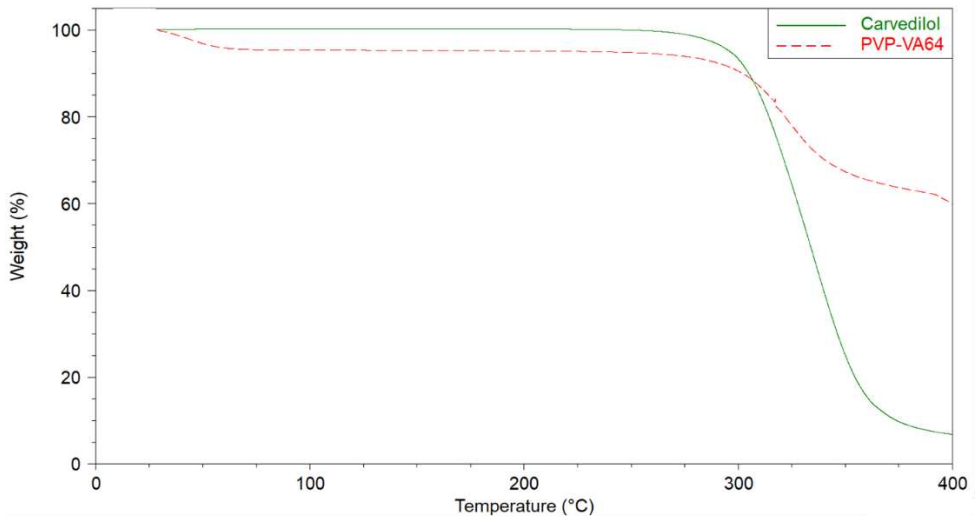

Figure 1. TGA graph of bulk VA64 and bulk CVD.

As shown in Figure 2, for bulk materials, CVD presented a melting endothermic peak at 119.82 °C [32]. VA64 exhibited a glass transition at 102.72 °C [33]. Previous studies have demonstrated the significant importance of studying thermal events of bulk materials for print process optimisation [34]. The environment and build plate temperatures during the printing process must be kept below the melting point or glass transition of the component with the lowest value to avoid melting of the blend prior to laser radiation. Herein the environment printing temperature was maintained below the glass transition of VA64.

Preprints (www.preprints.org) | NOT PEER-REVIEWED | Posted: 5 July 2023 doi:10.20944/preprints202307.0202.v1

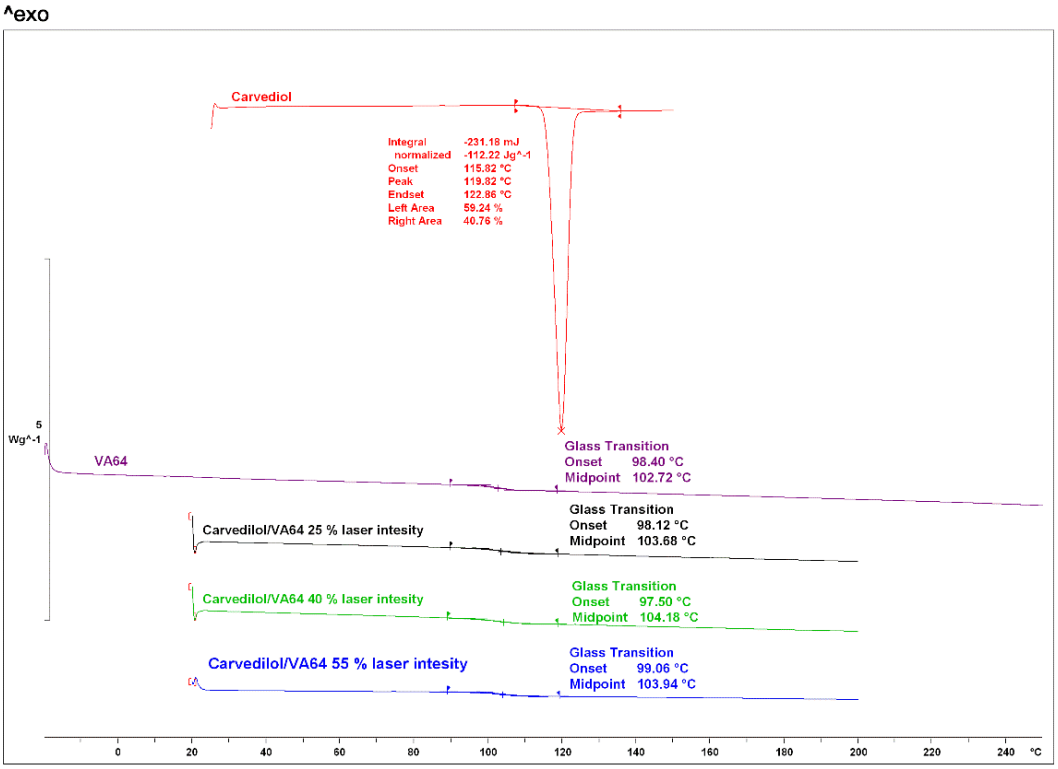

Figure 2. DSC thermograms of the bulk CVD, VA64 and 3-D printed tablets at different laser intensities.

3.2. Powder characterisation

The particle size distribution of the printing powder is a critical material attribute for the SLS technology, as it has been shown to greatly affect flowability and spreading [35]. The use of powder blends with adequate flowability ensures excellent spreading across the surface which in turn allows the formation of uniform layers during printing. As shown in Figure 3, the average particle size distribution for the drug blends was 81.2 μm. As reported in previous studies, the particle size of the powder was in a suitable range for printing [36,37]. In addition, the particle morphology of bulk VA64 appears spherical which is ideal for printing purposes. The flowability of the blends was determined using the Carr's Index; it was found to be 22.3. The good flowability is related to the flow properties of VA64. The presence of CVD in the blends had a negligible effect due to its low concentration in the final blends (3.125% and 6.25%).

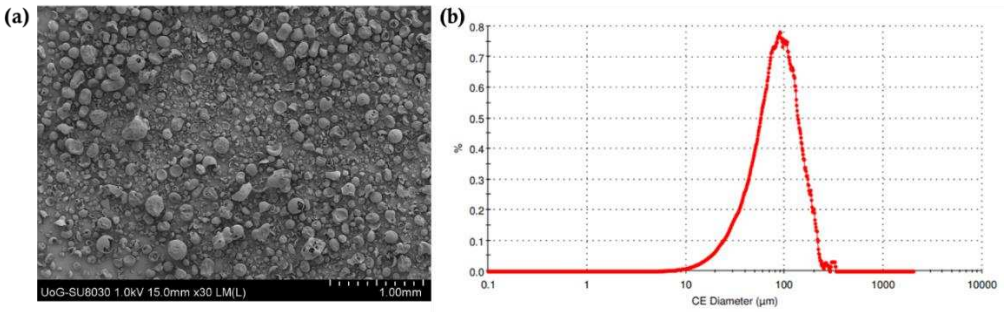

Figure 3. a) SEM image of the blend with 30x magnification and the (b) particle size distribution of the blend.

3.3. SLS for printing personalised dosage forms

 doi:10.20944/preprints202307.0202.v1

SLS printing uses laser radiation at temperatures close to the Tm or Tg of the polymers to fuse the thermoplastic particles. In a majority of the reported SLS studies where pharmaceutical dosage forms comprising of drug and polymer blends were manufactured, the blends did not absorb the laser light and prohibited the sintering process. As a result, Candurin gold sheen varying from 1-3% was added as a binder to improve printability. A major advantage of the current study was the use of CO2 laser (10.6 μm) due to its good absorptivity at lower applied energies. In addition, the CO2 printers are cost effective and present better printing precision in comparison to Nd:YAG lasers (λ = 1.064 μm). For the development of CVD personalised dosage forms, VA64 was selected as the polymer carrier due to its good flow properties, good sinterability, and high hydrophilicity. The VA64 flowability ensured adequate powder spreading throughout the layering step while the sinterability is related to the good VA64 absorption from the presence of -C-O- groups and powder flow [38,39].

For the print processing parameters, the bed temperature was set at 90°C, below the Tg and Tm of VA64 and CVD respectively. The laser speed was selected at 8,000 pps by applying a trial-and-error methodology. It has been previously reported that the laser speed affects the tablet porosity, where a lower speed results in a denser structure, and higher speeds produce less packed and porous tablets [40]. As shown in Table 1, the laser intensity was varied from 25-55% to investigate its effect on the tablet hardness, friability, and dissolution rates of the obtained tablets.

It was observed that by varying the laser intensity and tablet dimensions (e.g., thickness) the shape and geometry of the printed structures was not affected. As shown in Figure 4, when tablets were printed at lower intensities, the external shell presented a lighter density and a light colour, while a dark yellowish colour was observed for the inner cores. The results observed by Cheah et al [41] showed the inner core of CVD/VA64 tablets appear denser by increasing the intensity from 25 to 55%. These results are contradictory to Cheah as the sintering process, which uses a CO2 laser, takes place through the melting of the VA64 polymer capturing the neighbouring unmolten particles on the surface of the sintered layers. The formation of non-porous printed tablets with increasing laser intensity was also observed by SEM analysis as illustrated in Figure 5. It was observed that the CVD/VA64 particles are completely molten and the tablet cores appear entirely fused with minimal visible voids. By altering the laser intensity and the sintering process, denser tablets can be manufactured which in turn influences the tablet physicochemical and mechanical properties.

Preprints (www.preprints.org) | NOT PEER-REVIEWED | Posted: 5 July 2023 doi:10.20944/preprints202307.0202.v1

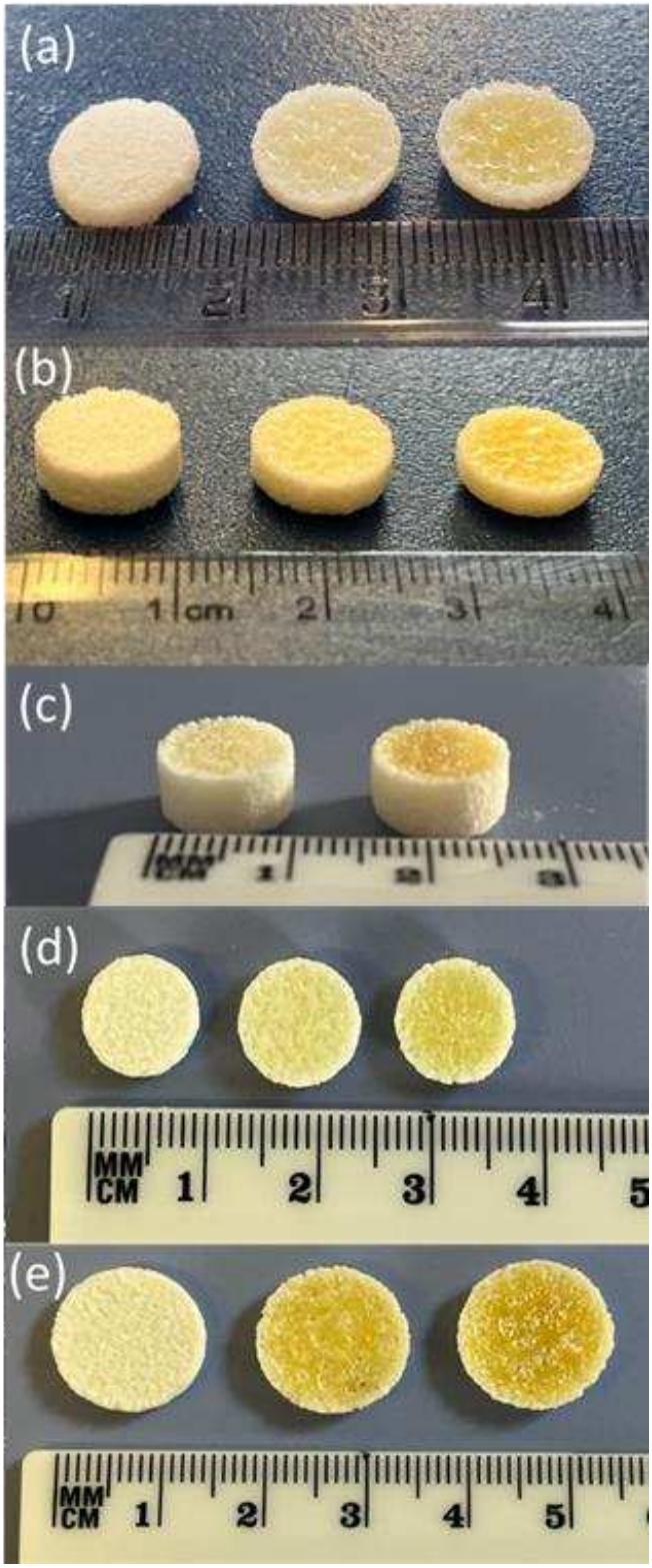

Figure 4. 3D printed tablets with different laser intensities (a) 100 mg (laser intensity from left to right respectively: 25, 40 and 55%) (b) 200 mg (laser intensity from left to right respectively: 25, 40 and 55%) and (c) 400 mg using 3.125% CVD blend (laser intensity from left to right respectively: 40 and 55%). 3D printed tablets printed with different laser intensities (d) 100 mg (laser intensity from left to right respectively: 25, 40 and 55%) and (e) 200 mg (laser intensity from left to right respectively: 25, 40 and 55%) with 6.25% loading.

Preprints (www.preprints.org) | NOT PEER-REVIEWED | Posted: 5 July 2023 doi:10.20944/preprints202307.0202.v1

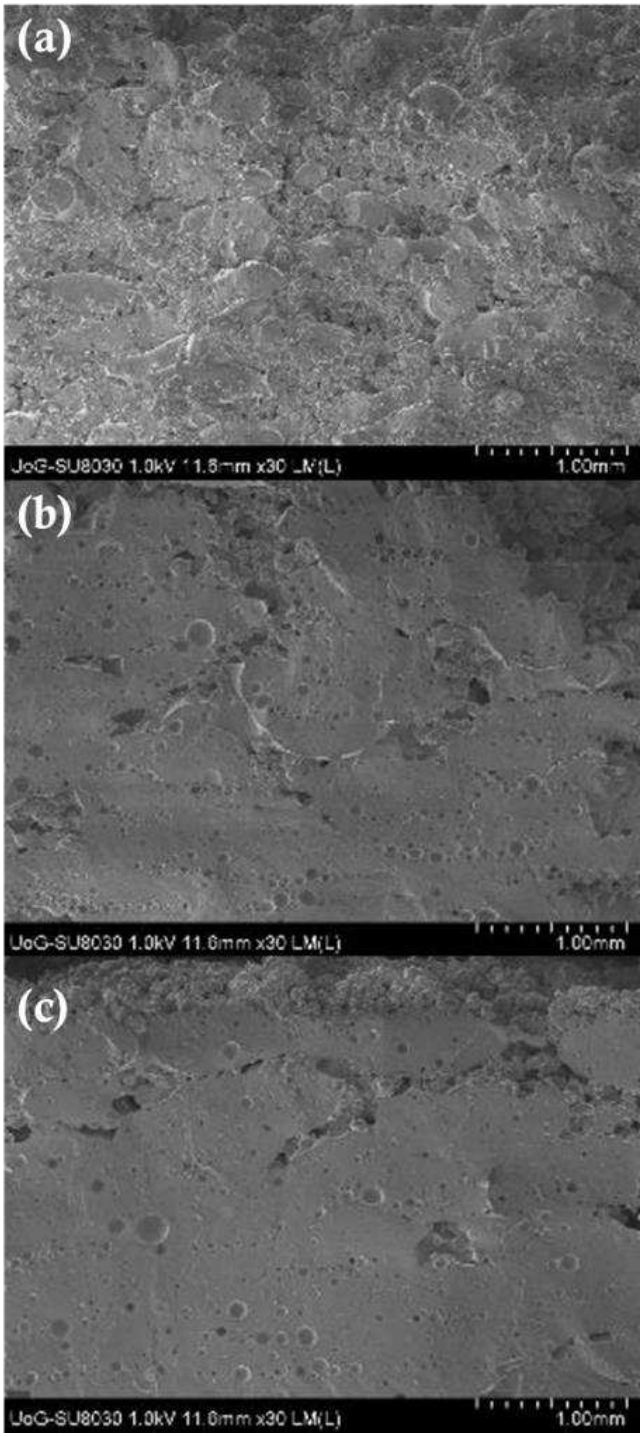

Figure 5. SEM images of the 3D printed tablets printed at (a) 25%, (b) 40% and (c) 55% laser intensities.

To print personalised CVD tablets, the active amount was adjusted by either altering the tablet weight (100-400 mg per tablet) using the same CVD/VA64 batch, or by increasing the CVD content from 3.125% to 6.25% in the powder blend. Table 1 presents the average weight, hardness, and friability of tablets printed at various laser intensities. The SLS printing process presented excellent reproducibility and accuracy. The weight variation for 200 mg and 400 mg tablets was less than 1% and 2% respectively. The tablet hardness increased from 98 – 208 N with increasing laser intensity. It was observed that tablet hardness was also increased with increasing tablet weight. For example, by applying the same laser intensity (40%) and CVD content (12.6 mg) the average hardness for the 400 mg tablets was 105.4 N vs. 35.9 N for 200 mg tablets.

Preprints (www.preprints.org) | NOT PEER-REVIEWED | Posted: 5 July 2023 doi:10.20944/preprints202307.0202.v1

The tablet friability was inversely proportional to the laser intensity and decreased by increasing the applied radiation. The estimated friability was attributed to the outer tablet walls in which the powder particles are fully sintered. Nevertheless, all tablet batches were easy to handle and did not break freely when transferred.

Table 2. Physical and mechanical properties of 3D printed CVD tablets at various CVD doses and laser intensities.

Theoretical tablet weight (mg)	100			200			400		100			200		
Theoretical CVD (mg)	3.125			6.25			12.5		6.25			12.5		
Laser intensity (%)	25	40	55	25	40	55	40	55	25	40	55	25	40	55
Average weight (mg)	98.5	101.3	103.4	210.8	209.4	205.8	403.2	405.4	102.3	103.5	101.3	207.5	204.5	208.2
Hardness (N)	10	18	24	36.5	80.6	95.2	105.4	125.5	11.4	19.5	26.9	13.5	35.9	47.6
Friability (%)	10.97	1.03	0.75	14.3	1.14	0.86	1.36	0.95	11.43	0.98	0.82	12.7	1.08	0.89
Weigh variation (±%)	<1	<1	<1	<1	<1	<1	<2	<2	<1	<1	<1	<1	<1	<1

3.4. Physiochemical characterisation of the 3D printed tablets

DSC and XRD were utilised to investigate the physical state of CVD within the 3D printed tablets. As shown in Figure 6, VA64 XRD showed no peaks due to its amorphous nature, while bulk CVD was in a crystalline state and diffraction peaks appeared at 5.8°, 11.5°, 13.0°, 14.8°, 16.3°, 17.4°, 18.4°, 24.2 ° and 29.3°/2θ. The characteristic diffraction peaks of CVD within the VA64 physical blend (3.125% CVD loading) show the drug was in a crystalline form prior to printing. X-ray diffractograms of CVD blends post SLS at different laser intensities showed haloes, indicating the absence of CVD crystallinity. To the best of our knowledge, only Madžarević et al., has reported the transformation of an API into an amorphous state as a result of SLS processing for the formation of printed tablets [42]. The findings suggest that for the polymer and drug used in this study, SLS printing of solid dosage forms may be able to produce an amorphous solid dispersion increasing the apparent solubility of the API [43]. The applicability of this technology to different drugs and higher drug loads warrants further investigation.

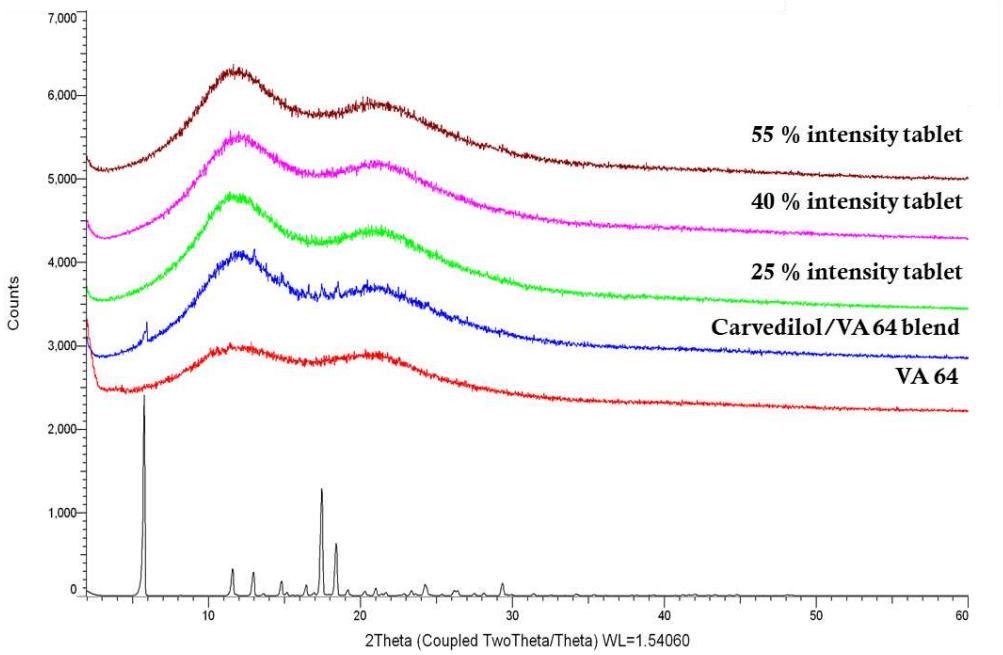

Preprints (www.preprints.org) | NOT PEER-REVIEWED | Posted: 5 July 2023 doi:10.20944/preprints202307.0202.v1

Figure 6. XRD graphs of the bulk materials printing physical blend (3.125% CVD loading) and the respective tablets 3D printed at different laser intensities.

3.5. Volumetric characterisation by means of X-ray μCT

As shown in Figure 7, μCT analysis was carried out to further investigate the properties of the printed tablets. The experimental findings showed that the total volume, total porosity, micro- and macro-porosity of the samples varied significantly between the specimens printed at 25% laser intensity, in comparison to those printed at 40% and 55% respectively.

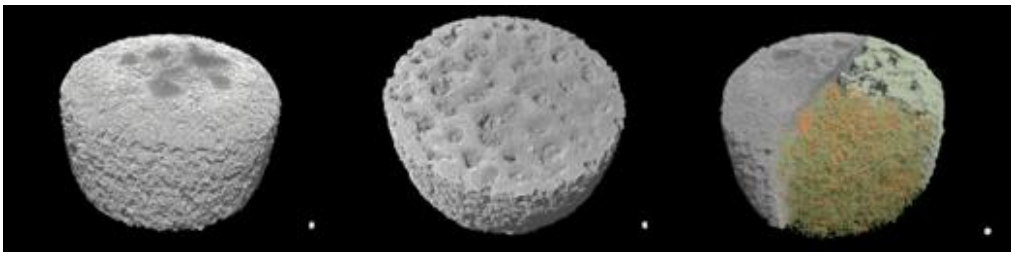

Figure 7. 3D volume renderings of the SLS printed specimens from different views. The top and bottom views are displayed on the left and middle, respectively. On the right, a clipped top view is shown, which reveals both macroporosity and microporosity. Specifically, the top portion of the clipped region is selectively rendered to display macroporosity, while the bottom portion displays microporosity.

Figure 8 shows the total, micro- and macro porosity for tablets at different laser intensities. The total volume (including pores space) of the samples printed at 55% and 40% laser intensity were 449.25 mm3 and 449.76 mm3 respectively, with both presenting similar total porosities at approximately 22%. The tablet printed at a 25% laser intensity was marginally larger at 466.05 mm3 (including pores space) but the total porosity was measured at 28.4%. While the total porosity varied for the different laser intensities, the micro-porosity remained unchanged at approximately 6.6-7.0%. These results indicate that the laser power-depended porosity-change is dominated and driven by changes in the macro-porosity, which is better visualised in Figure 9.

Preprints (www.preprints.org) | NOT PEER-REVIEWED | Posted: 5 July 2023 doi:10.20944/preprints202307.0202.v1

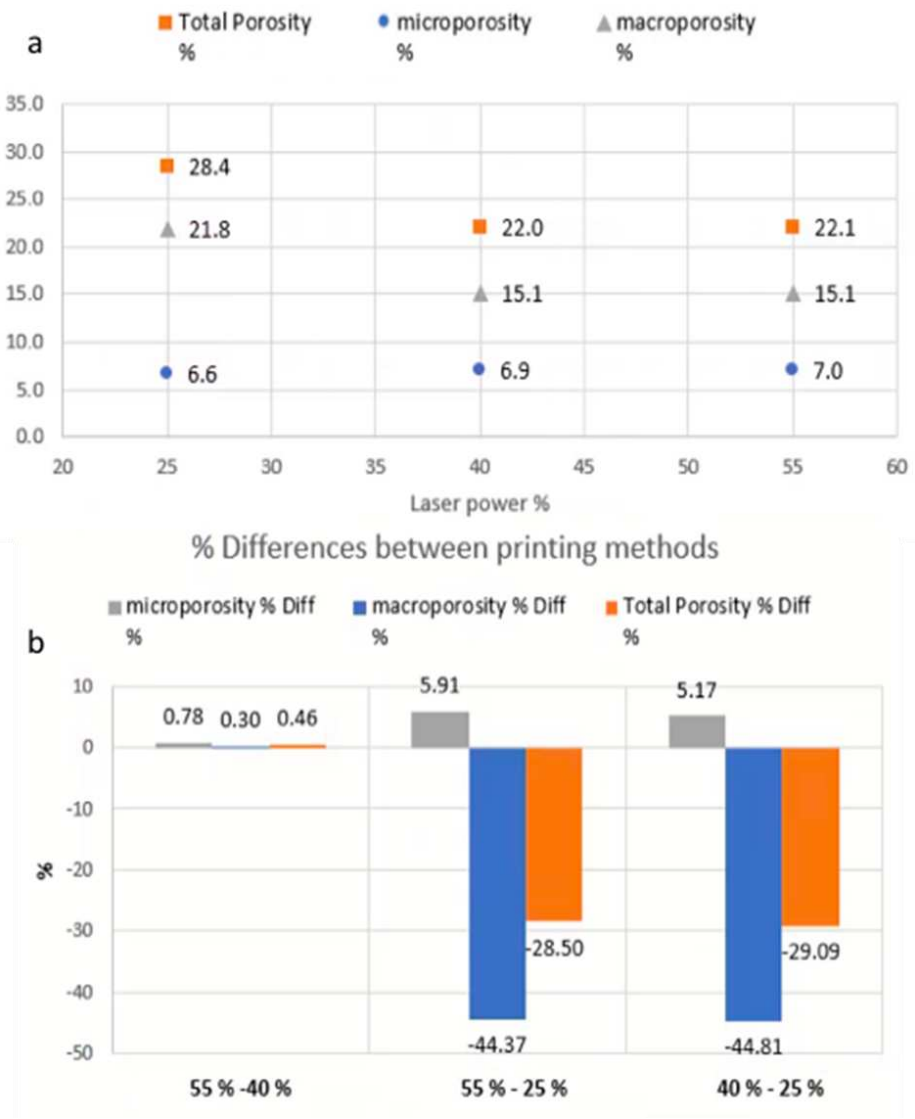

Figure 8. Porosity quantification. (a) Total porosity percentage, and its constituent component of micro- and microporosity resulted at different laser-power. (b) Total porosity, microporosity and macroporosity difference between the different laser-power printings.

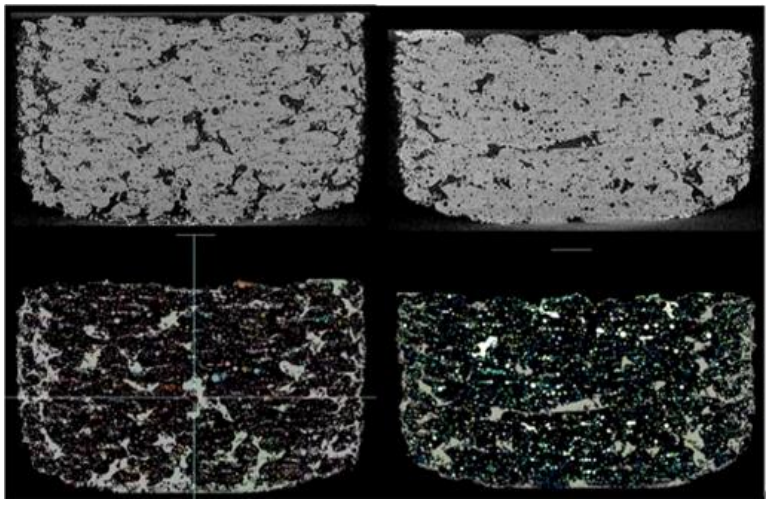

 doi:10.20944/preprints202307.0202.v1

Figure 9. (Top row) A single slice displaying the structure and porosity of a component printed with 25% laser intensity on the left and another component printed with 55% laser intensity on the right. (Bottom row) Macroporosity (in green) and microporosity (multicolour).

3.6. Release studies

The SLS printed tablets at different laser intensities and dosage strengths comprising of 3.125, 6.25, and 12.5 mg were investigated for their dissolution rates. According to the US Pharmacopeia, the dissolution rate of CVD active doses should be no less than 80% within 30 min. Figure 10a–e show the dissolution curves for all printed tablet batches. For the 3.125 mg strength (100 mg tablet weight) with a 3.125% drug loading, (Figure 10 the dissolution rates met the required specifications at all laser intensities. Figure 10b and c show the dissolution rates for 6.25 mg (200 mg tablet weight) and 12.5 mg (400 mg tablet weight) strength tablets using the same 3.125% drug loading. As the dose, and therefore tablet weight increased, the dissolution rate and total amount of drug released decreased. For the 6.25 mg tablet, CVD dissolution rates varied from 40-60% depending on laser intensity (Figure 10b). For the 12.5 mg, the dissolution rate was around 20% after 60 min (Figure 10c). It was evident that by proportionally increasing the tablet weight (thicker tablets) and the CVD active dose, a slower release was obtained due to the denser structure of the tablets. As a result, the slow VA64 erosion rate determined the CVD dissolution rates.

Preprints (www.preprints.org) | NOT PEER-REVIEWED | Posted: 5 July 2023 doi:10.20944/preprints202307.0202.v1

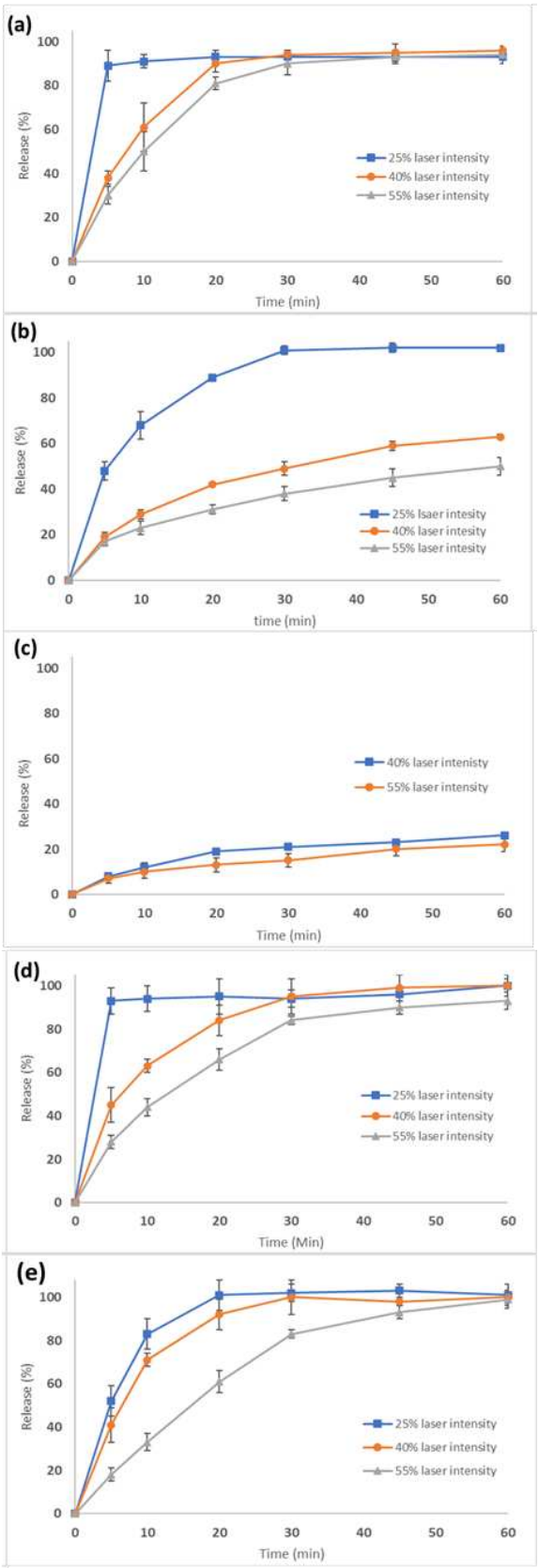

Figure 10. Dissolution rates of tablets of various strengths printed at different laser intensities. (a) 3.125 mg, (b) 6.25, (c)12.5, (d) 6.5 and (e) 12.5 mg strengths.

To improve the dissolution rate for the higher dosage strengths, the drug loading in the CVD/VA 64 formulation was increased to 6.25%. With a total tablet weight of 100 mg, tablets were printed at

Preprints (www.preprints.org) | NOT PEER-REVIEWED | Posted: 5 July 2023 doi:10.20944/preprints202307.0202.v1

various laser intensities. As shown in Figure 10d, the tablets printed at 40-55% laser intensities presented slower rates in the first 20 min compared to those printed at 25%. However, the CVD concentration was greater than 80% after 30 min for all printed tablets.

Based on these results, the tablet diameter of the 12.5 mg tablet was increased from 10 to 13 mm to maintain the same tablet thickness as the 6.25 mg tablet. It was thought that by maintaining the same surface to volume ratio, the dissolution rate of the 12.5 mg tablet would increase [18,44]. As shown in Figure 10e, all three formulations (F12-14) had greater than 80% released in 30 min, meeting USP specifications.

Table 3 summarizes the SLS printed tablets dissolution, friability, and hardness for various CVD doses processed at different laser intensities. The results demonstrate that SLS can be used for the design and printing of personalized dosage forms. Moreover, it is feasible to produce all CVD dose strengths in one print cycle by varying the laser intensity and the formulation composition.

Table 3. Friability and dissolution rate acceptability of the 3D printed CVD tablets at different.

Tablet weight (mg)	100			200			400		100			200		
CVD (mg)	3.125			6.25			12.5		6.25			12.5		
Tablet formulation	F1	F2	F3	F4	F5	F6	F7	F8	F9	F10	F11	F12	F13	F14
Dissolution	✓	✓	✓	✓	x	x	x	x	✓	✓	✓	✓	✓	✓
Friability	x	✓	✓	x	✓	✓	✓	✓	x	✓	✓	x	✓	✓

* The check marks mean that the tablets meet a) the pharmacopeia specifications in terms of dissolution and b) friability is <1%.

4. Conclusions

Selective laser sintering has been employed for the design and manufacturing of CVD personalised dosage forms at various strengths. It was feasible to print tablets of three different strengths that fulfil the required pharmacopeia specifications. Modulating the applied laser intensity impacted the tablet quality characteristics including tablet hardness, friability, dissolution rate, and total amount of drug released. An increased laser intensity produced a denser tablet resulting in a slower release rate, total amount of drug released over the course of 90 minutes, increased tablet hardness, and decreased friability.

This SLS study highlights many potential applications and exemplifies the use of this technology for the manufacturing of personalised dosage forms, especially for point of care services. First, it is feasible that laser intensity could be used to tailor and modify the release rate of a drug producing an extended or sustained released effect. Second, SLS was able to manufacture a tablet that did not contain a detectable amount of crystalline drug substance. While the stability of this apparently amorphous drug product was not studied, this technique could be a viable technology to quickly generate amorphous drug product without the need to generate extensive stability or go through time consuming and cumbersome manufacturing steps. This could quicken the time to clinic for drug substance candidates which are known to need an amorphous form to improve exposure.

Author Contributions: For research articles with several authors, a short paragraph specifying their individual contributions must be provided. The following statements should be used "Conceptualization, AGT. and DD.; methodology, AGT. and DD; validation, AGT. and DD..; formal analysis, AGT. and DD; investigation, AGT. QGM, AB, VG, RF, BN, JJ, SN and DD.; data curation, AGT. and DD.; writing—original draft preparation, AGT,and DD; writing—review and editing, AGT, NB and DD supervision, DD.; project administration, D.D.;. All authors have read and agreed to the published version of the manuscript."

Funding: Please add:

References

1. Barbosa, W.S.; Wanderley, R.F.F.; Gioia, M.M.; Gouvea, F.C.; Gonçalves, F.M. Additive or subtractive manufacturing: Analysis and comparison of automotive spare-parts. *J. Remanufacturing* 2022, doi:10.1007/s13243-021-00106-1.
2. Tabriz, A.G.; Hermida, M.A.; Leslie, N.R.; Shu, W. Three-dimensional bioprinting of complex cell laden alginate hydrogel structures. *Biofabrication* 2015, *7*, 45012, doi:10.1088/1758-5090/7/4/045012.
3. Madhavadas, V.; Srivastava, D.; Chadha, U.; Aravind Raj, S.; Sultan, M.T.H.; Shahar, F.S.; Shah, A.U.M. A review on metal additive manufacturing for intricately shaped aerospace components. *CIRP J. Manuf. Sci. Technol.* 2022, *39*, 18–36, doi:https://doi.org/10.1016/j.cirpj.2022.07.005.
4. Andreadis, I.I.; Gioumouxouzis, C.I.; Eleftheriadis, G.K.; Fatouros, D.G. The Advent of a New Era in Digital Healthcare: A Role for 3D Printing Technologies in Drug Manufacturing? *Pharm.* 2022, *14*.
5. Menano, L.; Fidalgo, P.; Santos, I.M.; Thormann, J. Integration of 3D Printing in Art Education: A Multidisciplinary Approach. *Comput. Sch.* 2019, doi:10.1080/07380569.2019.1643442.
6. Chai, X.; Chai, H.; Wang, X.; Yang, J.; Li, J.; Zhao, Y.; Cai, W.; Tao, T.; Xiang, X. Fused Deposition Modeling (FDM) 3D Printed Tablets for Intragastric Floating Delivery of Domperidone. *Sci. Rep.* 2017, *7*, 2829, doi:10.1038/s41598-017-03097-x.
7. Abdelki, A. Fused deposition modeling of API-loaded mesoporous magnesium carbonate, Nanotechnology and Functional Materials, Department of Materials Science and Engineering, Technology, Disciplinary Domain of Science and Technology, Uppsala University, 2020, Vol. Independen.
8. Tabriz, A.G.; Mithu, M.S.; Antonijevic, M.D.; Vilain, L.; Derrar, Y.; Grau, C.; Morales, A.; Katsamenis, O.L.; Douroumis, D. 3D printing of LEGO® like designs with tailored release profiles for treatment of sleep disorder. *Int. J. Pharm.* 2023, *632*, 122574, doi:https://doi.org/10.1016/j.ijpharm.2022.122574.
9. Iftimi, L.-D.; Edinger, M.; Bar-Shalom, D.; Rantanen, J.; Genina, N. Edible solid foams as porous substrates for inkjet-printable pharmaceuticals. *Eur. J. Pharm. Biopharm.* 2019, *136*, 38–47, doi:https://doi.org/10.1016/j.ejpb.2019.01.004.
10. Awad, A.; Fina, F.; Goyanes, A.; Gaisford, S.; Basit, A.W. 3D printing: Principles and pharmaceutical applications of selective laser sintering. *Int. J. Pharm.* 2020, *586*, 119594, doi:10.1016/j.ijpharm.2020.119594.
11. Wang, J.; Goyanes, A.; Gaisford, S.; Basit, A.W. Stereolithographic (SLA) 3D printing of oral modified-release dosage forms. *Int. J. Pharm.* 2016, *503*, 207–212, doi:https://doi.org/10.1016/j.ijpharm.2016.03.016.
12. Boniatti, J.; Januskaite, P.; da Fonseca, L.B.; Viçosa, A.L.; Amendoeira, F.C.; Tuleu, C.; Basit, A.W.; Goyanes, A.; Ré, M.I. Direct powder extrusion 3d printing of praziquantel to overcome neglected disease formulation challenges in paediatric populations. *Pharmaceutics* 2021, doi:10.3390/pharmaceutics13081114.
13. Tabriz, A.G.; Nandi, U.; Scoutaris, N.; Sanfo, K.; Alexander, B.; Gong, Y.; Hui, H.-W.; Kumar, S.; Douroumis, D. Personalised paediatric chewable Ibuprofen tablets fabricated using 3D micro-extrusion printing technology. *Int. J. Pharm.* 2022, *626*, 122135, doi:https://doi.org/10.1016/j.ijpharm.2022.122135.
14. Zhang, J.; Feng, X.; Patil, H.; Tiwari, R. V; Repka, M.A. Coupling 3D printing with hot-melt extrusion to produce controlled-release tablets. *Int. J. Pharm.* 2017, *519*, 186–197, doi:https://doi.org/10.1016/j.ijpharm.2016.12.049.
15. Tan, Y.J.N.; Yong, W.P.; Kochhar, J.S.; Khanolkar, J.; Yao, X.; Sun, Y.; Ao, C.K.; Soh, S. On-demand fully customizable drug tablets via 3D printing technology for personalized medicine. *J. Control. Release* 2020, doi:10.1016/j.jconrel.2020.02.046.
16. Goyanes, A.; Robles Martinez, P.; Buanz, A.; Basit, A.W.; Gaisford, S. Effect of geometry on drug release from 3D printed tablets. *Int. J. Pharm.* 2015, *494*, 657–663, doi:https://doi.org/10.1016/j.ijpharm.2015.04.069.
17. Bangalore, S.; Kamalakkannan, G.; Parkar, S.; Messerli, F.H. Fixed-Dose Combinations Improve Medication Compliance: A Meta-Analysis. *Am. J. Med.* 2007, *120*, 713–719, doi:https://doi.org/10.1016/j.amjmed.2006.08.033.
18. Tabriz, A.G.; Fullbrook, D.H.; Vilain, L.; Derrar, Y.; Nandi, U.; Grau, C.; Morales, A.; Hooper, G.; Hiezl, Z.; Douroumis, D. Personalised Tasted Masked Chewable 3D Printed Fruit-Chews for Paediatric Patients. *Pharm.* 2021, *13*.
19. Tabriz, A.G.; Nandi, U.; Scoutaris, N.; Sanfo, K.; Alexander, B.; Gong, Y.; Hui, H.-W.; Kumar, S.; Douroumis, D. Personalised paediatric chewable Ibuprofen tablets fabricated using 3D micro-extrusion printing technology. *Int. J. Pharm.* 2022, *626*, 122135, doi:https://doi.org/10.1016/j.ijpharm.2022.122135.
20. Ghanizadeh Tabriz, A.; Nandi, U.; Hurt, A.P.; Hui, H.-W.; Karki, S.; Gong, Y.; Kumar, S.; Douroumis, D. 3D Printed Bilayer Tablet with Dual Controlled Drug Release for Tuberculosis Treatment. *Int. J. Pharm.* 2020, 120147, doi:https://doi.org/10.1016/j.ijpharm.2020.120147.
21. Robles-Martinez, P.; Xu, X.; Trenfield, S.J.; Awad, A.; Goyanes, A.; Telford, R.; Basit, A.W.; Gaisford, S. 3D Printing of a Multi-Layered Polypill Containing Six Drugs Using a Novel Stereolithographic Method. *Pharm.* 2019, *11*.
22. Khaled, S.A.; Burley, J.C.; Alexander, M.R.; Yang, J.; Roberts, C.J. 3D printing of five-in-one dose combination polypill with defined immediate and sustained release profiles. *J. Control. Release* 2015, *217*, 308–314, doi:https://doi.org/10.1016/j.jconrel.2015.09.028.

23. Gryczke, A.; Schminke, S.; Maniruzzaman, M.; Beck, J.; Douroumis, D. Development and evaluation of orally disintegrating tablets (ODTs) containing Ibuprofen granules prepared by hot melt extrusion. *Colloids Surf. B. Biointerfaces* 2011, *86*, 275–284, doi:10.1016/j.colsurfb.2011.04.007.
24. Ponsar, H.; Wiedey, R.; Quodbach, J. Hot-melt extrusion process fluctuations and their impact on critical quality attributes of filaments and 3d-printed dosage forms. *Pharmaceutics* 2020, doi:10.3390/pharmaceutics12060511.
25. Xu, P.; Li, J.; Meda, A.; Osei-Yeboah, F.; Peterson, M.L.; Repka, M.; Zhan, X. Development of a quantitative method to evaluate the printability of filaments for fused deposition modeling 3D printing. *Int. J. Pharm.* 2020, *588*, 119760, doi:https://doi.org/10.1016/j.ijpharm.2020.119760.
26. Elbadawi, M.; Gustaffson, T.; Gaisford, S.; Basit, A.W. 3D printing tablets: Predicting printability and drug dissolution from rheological data. *Int. J. Pharm.* 2020, *590*, 119868, doi:https://doi.org/10.1016/j.ijpharm.2020.119868.
27. Fina, F.; Goyanes, A.; Gaisford, S.; Basit, A.W. Selective laser sintering (SLS) 3D printing of medicines. *Int. J. Pharm.* 2017, *529*, 285–293, doi:https://doi.org/10.1016/j.ijpharm.2017.06.082.
28. Fina, F.; Goyanes, A.; Madla, C.M.; Awad, A.; Trenfield, S.J.; Kuek, J.M.; Patel, P.; Gaisford, S.; Basit, A.W. 3D printing of drug-loaded gyroid lattices using selective laser sintering. *Int. J. Pharm.* 2018, *547*, 44–52, doi:https://doi.org/10.1016/j.ijpharm.2018.05.044.
29. Gueche, Y.A.; Sanchez-Ballester, N.M.; Bataille, B.; Aubert, A.; Leclercq, L.; Rossi, J.-C.; Soulairol, I. Selective Laser Sintering of Solid Oral Dosage Forms with Copovidone and Paracetamol Using a CO2 Laser. *Pharm.* 2021, *13*.
30. Rele, R. V.; Tiwatane, P.P. UV spectrophotometric estimation of carvedilol hydrochloride by second order derivative methods in bulk and pharmaceutical dosage form. *Res. J. Pharm. Technol.* 2014.
31. Beattie, K.; Phadke, G.; Novakovic, J. Carvedilol. In *Profiles of Drug Substances, Excipients and Related Methodology*; 2013.
32. Fernandes, G.J.; Rathnanand, M.; Kulkarni, V. Mechanochemical Synthesis of Carvedilol Cocrystals Utilizing Hot Melt Extrusion Technology. *J. Pharm. Innov.* 2019, *14*, 373–381, doi:10.1007/s12247-018-9360-y.
33. Wang, X.; Michoel, A.; Van den Mooter, G. Solid state characteristics of ternary solid dispersions composed of PVP VA64, Myrj 52 and itraconazole. *Int. J. Pharm.* 2005, *303*, 54–61, doi:https://doi.org/10.1016/j.ijpharm.2005.07.002.
34. Kulinowski, P.; Malczewski, P.; Łaszcz, M.; Baran, E.; Milanowski, B.; Kuprianowicz, M.; Dorożyński, P. Development of Composite, Reinforced, Highly Drug-Loaded Pharmaceutical Printlets Manufactured by Selective Laser Sintering—In Search of Relevant Excipients for Pharmaceutical 3D Printing. *Materials (Basel).* 2022, *15*.
35. Bai, J.; Zhang, B.; Song, J.; Bi, G.; Wang, P.; Wei, J. The effect of processing conditions on the mechanical properties of polyethylene produced by selective laser sintering. *Polym. Test.* 2016, doi:10.1016/j.polymertesting.2016.04.004.
36. Goodridge, R.D.; Tuck, C.J.; Hague, R.J.M. Laser sintering of polyamides and other polymers. *Prog. Mater. Sci.* 2012.
37. Meier, C.; Weissbach, R.; Weinberg, J.; Wall, W.A.; Hart, A.J. Critical influences of particle size and adhesion on the powder layer uniformity in metal additive manufacturing. *J. Mater. Process. Technol.* 2019, *266*, 484–501, doi:https://doi.org/10.1016/j.jmatprotec.2018.10.037.
38. Salmoria, G. V.; Klauss, P.; Zepon, K.; Kanis, L.A.; Roesler, C.R.M.; Vieira, L.F. Development of functionally-graded reservoir of PCL/PG by selective laser sintering for drug delivery devices: This paper presents a selective laser sintering-fabricated drug delivery system that contains graded progesterone content. *Virtual Phys. Prototyp.* 2012, doi:10.1080/17452759.2012.687911.
39. Gueche, Y.A.; Sanchez-Ballester, N.M.; Bataille, B.; Aubert, A.; Leclercq, L.; Rossi, J.C.; Soulairol, I. Selective laser sintering of solid oral dosage forms with copovidone and paracetamol using a CO2 laser. *Pharmaceutics* 2021, doi:10.3390/pharmaceutics13020160.
40. Fina, F.; Madla, C.M.; Goyanes, A.; Zhang, J.; Gaisford, S.; Basit, A.W. Fabricating 3D printed orally disintegrating printlets using selective laser sintering. *Int. J. Pharm.* 2018, *541*, 101–107, doi:10.1016/J.IJPHARM.2018.02.015.
41. Cheah, C.M.; Leong, K.F.; Chua, C.K.; Low, K.H.; Quek, H.S. Characterization of microfeatures in selective laser sintered drug delivery devices. *Proc. Inst. Mech. Eng. Part H J. Eng. Med.* 2002, doi:10.1243/095441102321032166.
42. Madžarević, M.; Medarević, Đ.; Pavlović, S.; Ivković, B.; Đuriš, J.; Ibrić, S. Understanding the effect of energy density and formulation factors on the printability and characteristics of SLS Irbesartan tablets—application of the decision tree model. *Pharmaceutics* 2021, doi:10.3390/pharmaceutics13111969.
43. Maniruzzaman, M.; Rana, M.M.; Boateng, J.S.; Mitchell, J.C.; Douroumis, D. Dissolution enhancement of poorly water-soluble APIs processed by hot-melt extrusion using hydrophilic polymers. *Drug Dev. Ind. Pharm.* 2013, doi:10.3109/03639045.2012.670642.

44. Martinez, P.R.; Goyanes, A.; Basit, A.W.; Gaisford, S. Influence of Geometry on the Drug Release Profiles of Stereolithographic (SLA) 3D-Printed Tablets. *AAPS PharmSciTech* 2018, *19*, 3355–3361, doi:10.1208/s12249-018-1075-3.